Chemical Physics 575 (2023) 112043

Contents lists available at ScienceDirect

Chemical Physics

journal homepage: www.elsevier.com/locate/chemphys

Novel electrolytes based on mixtures of dimethyl sulfoxide task specific zwitterionic ionic liquid and lithium salts: Synthesis and conductivity studies

Daniel Nuevo [b], Marc Cuesta [b], Raul Porcar [b,d], Andreu Andrio [c], Eduardo Garcia-Verdugo [b], Vicente Compañ [a,*]

[a] Dpto. de Termodinámica Aplicada, Universitat Politècnica de Valencia, C/Camino de Vera s/n, Valencia 46020, Spain
[b] Dpto. Química Inorgánica y Orgánica, Universidad Jaume I, Avda. Sos, Baynat s/n, Castellón 12071, Spain
[c] Dpto. Física. Universidad Jaume I, Avda. Sos, Baynat s/n, Castellón 12071, Spain
[d] Dpto. de Química Orgánica y Bio-Orgánica, Facultad de Ciencias, UNED, E-28040 Avda. Esparta s/n, 28232 Las Rozas-Madrid, Spain

ARTICLE INFO

Keywords:
Ionic liquids
Electrochemical impedance spectroscopy
Conductivity
Ionic transport
Diffusivity

ABSTRACT

Novel methyl sulfoxide imidazolium-based zwitterionic low melting salts was synthesized and characterized. The combination of this functionalized zwitterion and lithium bis(trifluoromethylsulfonyl)amide ($LiNTf_2$) salts at different molar ratios of render to low melting mixtures, which can exhibit an ionic conductivity as high as 3.4×10^{-5} S cm^{-1} at 30 °C or 2.9×10^{-3} S cm^{-1} at 120 °C and a high thermal decomposition temperature higher than 250 °C. The thermal activation energy shown two clearly different Arrhenius trend. For all the mixtures the temperature where the slope of the Arrhenius plot changes is on the range of the melting temperature experimentally observed for the mixture. Below the melting temperature, the values of activation energy are around of two times higher than the values observed for all the mixtures above the melting temperature. On the other hand, in all the mixtures, we have observed that conductivity increases monotonically on the composition of the mixture. These non-volatile and highly polar novel materials can be used for the development of devices targeting high ionic Li-ion conductivity.

1. Introduction

Ionic liquids are systems solely formed by the combination of cations generally, of organic nature, and anions. The nature and structure of both cations and anions define their chemical and physical properties. ILs usually present a high ionic conductivity as they are molecules enterally form by ions. Therefore, they have huge potential to be used for electrochemical devices (i.e. electrolytes for rechargeable batteries and fuel cells). Zwitterionic ionic liquids (ZIs) have been envisioned as new electrolyte materials to achieve a high target-ion transference number [1,2].

In ZIs cation and anion are covalently tethered in a single molecule. Thus, in comparison with ILs, where both cation and anion present independent mobility when a potential gradient is applied, they can critically suppress the migration of the ions forming the ILs favouring the migration of the specific ion (i.e. lithium cations. protons. sodium cations. or iodide anions) added to them [3]. This can render to a higher Li^+ conductivity,when electrolytes based on zwitterionic ILs are used for electrical devices [4,5]. For this reason, different ZIs with certain degree of structural diversity have been designed and evaluated as electrolyte in conjunction with a variety of lithium salts (i.e. lithium bis(trifluoromethylsulfonyl)imide ($LiNTf_2$), lithium bis(perfluoroethylsulfonyl)imide (LiBETI), $LiBF_4$, $LiCF_3SO_3$ or $LiClO_4$) [6,7]. The presence of the lithium salt not only contributes to the ionic conductivity but also acts as a plasticizer reducing the melting point of the components of the mixture. The ionic conductivity of these mixtures is mainly governed by the interaction between both ionic components, especially the cationic moiety of ZI with the anion of the added salt. In general, higher ionic conductivity is reported when NTf_2 is used in comparison with other anions (i.e. BF_4^-, $CF_3SO_3^-$ ClO_4^-).

Task-specific ionic liquids are ILs containing a covalently tethered to one of both ions additional functional groups [8,9]. The presence of this specific functionality provides the ILs specific characteristics (i.e. acid, base, interaction with metal, etc.). In this regard, different authors have

* Corresponding authors at: Dpto. de Termodinámica Aplicada, Universitat Politècnica de Valencia, C/Camino de Vera s/n, Valencia 46020, Spain.
E-mail addresses: cepeda@uji.es (E. Garcia-Verdugo), vicommo@ter.upv.es (V. Compañ).

https://doi.org/10.1016/j.chemphys.2023.112043
Received 2 June 2023; Received in revised form 10 July 2023; Accepted 4 August 2023
Available online 9 August 2023

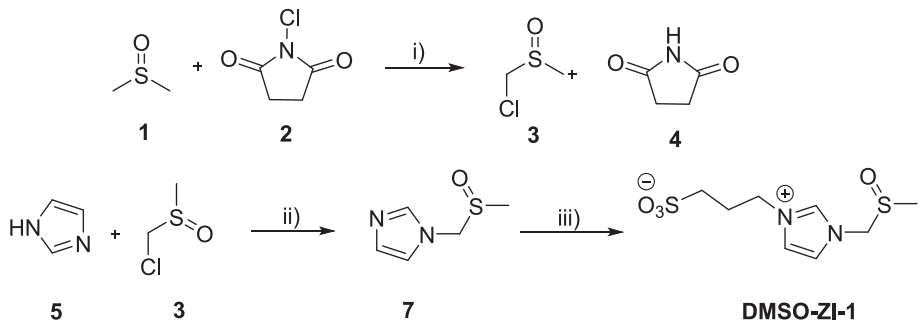

Scheme 1. Synthetic route of **DMSO-ZI-1**. i) K_2CO_4, KOH, CH_2Cl_2, 24 h, rt. ii) K_2CO_4, ACN, 30 min at 120 °C, 2 h at 90 °C; added **3** at 0 °C, 24 h, rt; KOH, 2 days, rt. iii) ACN, 1,3-propanesultone, 48 h, 35 °C.

Table 1
Composition and thermal behaviour of the mixtures **DMSO-ZI-1**:$LiNTf_2$ prepared.-

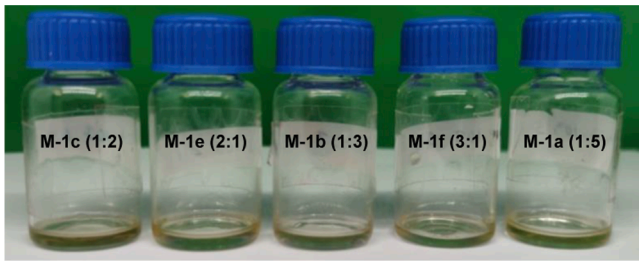

Entry	Mixture	x DMSO-ZI-1	x($LiNTf_2$)	T_m (°C)	T_d (°C)
1	**M-1a** (1:5)	0.17	0.83	37.5 ± 0.1	284 ± 5
2	**M-1b** (1:3)	0.25	0.75	36.9 ± 0.1	273 ± 5
3	**M-1c** (1:2)	0.33	0.67	36.4 ± 0.1	265 ± 5
4	**M-1d** (1:1)	0.50	0.50	57.3 ± 0.2	248 ± 5
5	**M-1e** (2:1)	0.67	0.33	60.4 ± 0.1	234 ± 5
6	**M-1f** (3:1)	0.75	0.25	60.7 ± 0.1	232 ± 5
7	**M-1g** (5:1)	0.83	0.17	64.3 ± 0.2	231 ± 5
8	**DMSO-ZI-1**	1	0	68.7 ± 0.2	220 ± 5

designed TSILs containing methyl sulfoxide moieties to be used in Swern oxidation of various benzylic and allylic alcohols suppressing the unpleasant smell of dimethylsulfide by-product of this reaction by reducing its volatility [10,11]. However, there is no reports, as far as we are aware, of the use of zwitterionic ionic liquids bearing methyl sulfoxide moieties, in a system that combined both the zweterionic unit and de S═O that can further solvate the Li cations to modulate the ionic conductivity of mixtures of ZI and lithium slats.

The presence of functional groups on the side chain of the cation presents a strong influence on the melting point of the ZI but also on their conductivities [2,3,5,6]. For instance, the presence of a flexible ethylene oxide unit and capable of interacting with ions are able effectively regardless of the anion structure of the zwitterion to reduce the ZÍs melting point increasing the conductivity as there is a good relationship between T_m and the ionic conductivity of the zwitterionic liquid/lithium salt mixtures [12].

Here, we reported the synthesis and properties of a task-specific-zwitterion ionic liquid functionalized with methyl sulfoxide moieties to form in the presence of $LiNTf_2$ eutectic mixtures. The resulting eutectic mixtures were analyzed and characterized by DSC, TGA, ATR-FT-IR spectroscopy, Raman spectroscopy and impedance spectroscopy. The conductivity of the resulting systems has been fully discussed and the free ion diffusivity and free ion charge density were obtained with the intention to quantify the concentration effect of the ZI in the mixture depending on its functionality.

2. Results and discussion

Synthesis and characterization of DMSO-ZIs and related eutectic mixtures. In order to prepare the task-specific zwitterionic salt 3-(1-((methylsulfinyl)methyl)-1H-imidazol-3-ium-3-yl)propane-1-sulfonate) (**DMSO**-ZI-1), first the functionalized imidazole (**7**) was obtained by alkylation of imidazole (**5**) with chloro(methylsulfinyl)methane (**3**). The compound **3** was prepared on large scale and good yield (90 %) by chlorination of DMSO (**1**) with chloro-*N*-succinimide (**2**) in the presence of a mixture of bases (Scheme 1). Finally, the reaction between imidazole **7** and 1.3-propane sultone led to the **DMSO**-ZI-1 obtained as a white solid. The thermal properties of this compound were analyzed by

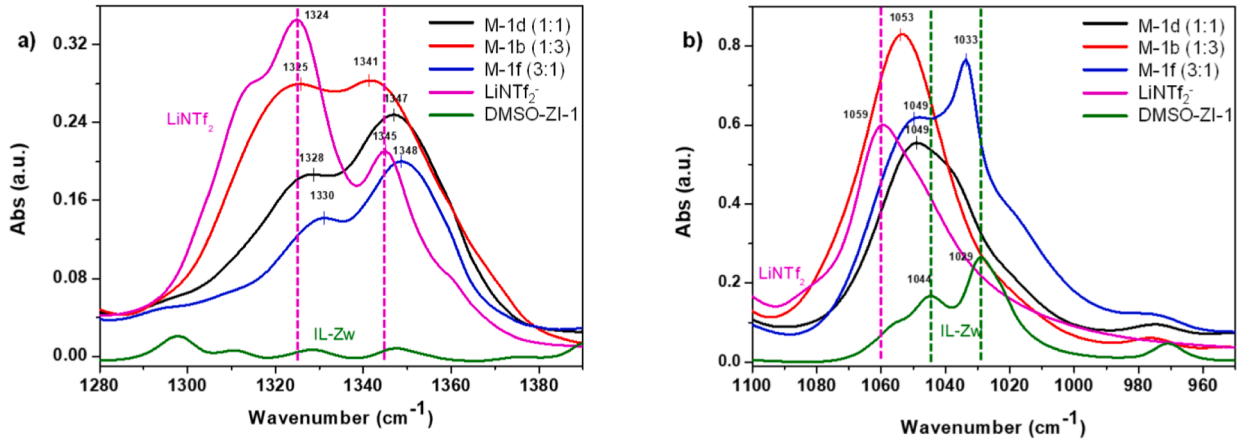

Fig. 1. Selected regions of the ATR-FT-IR spectra of **DMSO-ZI-1**, $LiNTf_2$ and different molar mixtures. The lines indicate the characteristic peak found for pure $LiNTf_2$ and **DMSO-ZI-1**. Samples Conductivity determinations. Temperature and frequency measurement process.

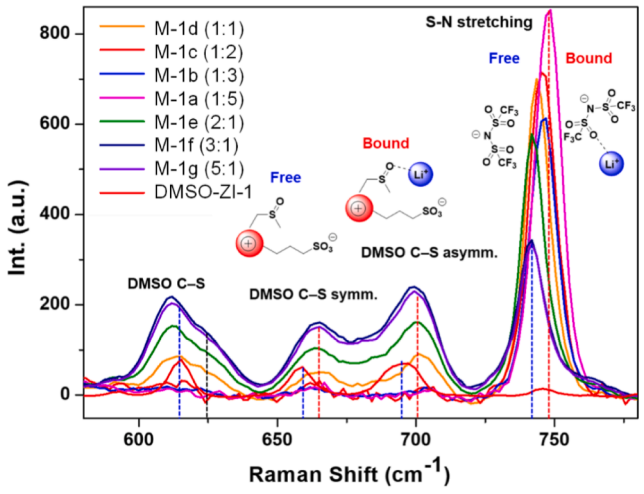

Fig. 2. Shows the Raman spectra (region 580–780 cm^{-1}) of the pure **DMSO-ZI-1** together with the different mixtures evaluated.

DSC and TGA (see Figure SI1 and Figure SI2). The DSC shows that **DMSO**-ZI-1 melts at 68.7 °C, while the TGA reveals that the ZI is thermally stable up to 235 °C.

Different mixtures of **DMSO**-ZI-1 with $LiNTf_2$ at a variety of molar ratios were prepared by solving both components in methanol followed by the evaporation of the solvent at high temperature (>120 °C) and under high vacuum to remove any trace of organic solvent (Table 1). In all the cases, the mixtures formed a molten salt due to the plastic effect of the bis(trifluoromethylsulfonyl)imide anion. The melting temperatures were lower than the ones for the individual components (see Table 1, and Figure SI3). The mixtures are wax materials at room temperature becoming, in all cases, liquid above 65 °C.

TGA experiments also showed that M-1e-g ($x_{ZIs\text{-}1} < 0.36$) decomposed at similar temperatures to **DMSO**-ZI-1 (ca. 230 °C), while mixtures with a larger amount of $LiNTf_2$ ($x_{LiNTf2} \geq 0.5$. **M**-1a-d) decomposed at higher temperatures 248 °C, 265 °C, 273 °C and 284 °C (Table 1 and Figure SI4).

The FT-IR-ATR of equimolecular mixture of **DMSO**-ZI-1 and $LiNTf_2$ shows that the band assignable to the asymmetric vibration of the SO_2 of the NTf_2 at near 1300 cm^{-1} shifts from 1325 cm^{-1} in bulk $LiNTf_2$ to lower frequencies with the presence of **DMSO-ZI-1** (1324, 1328 and 1320 cm^{-1} for **M-1b**, **M-1d** and **M-1f**, respectively, Fig. 1). A similar trend was also observed for the stretching vibration band associated with the C–F group at 1059 cm^{-1} for $LiNTf_2$. In this case, the observed shifts are a function of the composition of the **DMSO-ZI-1**:$LiNTf_2$ mixture. Thus, for an increase from 0.5 to 0.75 in the molar fraction of **DMSO-ZI-1** (**M-1d** and **M-1f**), the peak related to the symmetrical stretching peak of $–SO_2–N–SO_2–$ shifts to 1049 cm^{-1}, while lower shift observed for the mixture with higher $LiNTf_2$ content (from 1059 cm^{-1} to 1053 cm^{-1}). All these data suggest that in the mixtures the lithium cation is less coordinated to the NTf_2 anions by intermolecular interactions of the zwitterionic salt with the $LiNTf_2$ through hydrogen bonding. These interactions are likely to be the responsible of the reduction on the melting.

The zwitterionic IL not only provides the required interaction with the $LiNTf_2$ to reduce the melting point of the mixtures allowing easy handing but also affects the solvation of the Li in a similar fashion to the observed when DMSO is used as the electrolytic solvent. Raman can provide further information about the solvation of the zwitterionic ILs containing methyl sulfoxide moieties toward lithium ions in the binary mixtures prepared. Fig. 2 shows the Raman spectra (region 580–780 cm^{-1}) of the pure **DMSO-ZI-1** together with the different mixtures evaluated. The spectrum of **DMSO-ZI-1** showed three bands at 615, 658 and 697 cm^{-1}, which were assigned to the C—S symmetric and asymmetric stretching modes of S═O of the dimethylsulfoxide moiety of the **DMSO-ZI-1** [13]. Fortunately, these peaks do not overlap with any vibrational modes of $LiNTf_2$ providing information of this moiety across the different **DMSO-ZI-1**-$LiNTf_2$ formulation assayed. Indeed, in the mixtures these bands related to the S═O moieties are clearly split into two bands associated with the states of DMSO moiety: free and solvating DMSO. The newly observed bands at 623, 677 and 705 cm^{-1} can be assigned to the stretching modes of DMSO units that solvate lithium-ion (denoted as bound-DMSO at Fig. 2). A more intense scatter at the higher wavenumbers for the C—S—symmetric and asymmetric stretch of DMSO is detected with an increase in the amount of **DMSO-ZI-1** in the mixture. This suggests a solvation state of **DMSO-ZI-1** molecules with the lithium salt by the formation of clustering structures between the two components of the electrolytic mixtures. Indeed, the presence of the DMSO units in the zwitterionic ILs provides to similar solvating effect than those observed for DMSO/$LiNTf_2$ solutions [14]. The relative contribution of the free and bound S═O in the ZI to the Li^+ can be used to estimate the Li+ solvation number (n) of $[Li(ZI)_n]^+$ taking into account the intensities of these bands, which change linearly with the molar ratio of components of the mixture. Assuming that the Raman scattering coefficients for free and bound-DMSO were identical and constant in the whole concentration range the n can be calculated from $I_b/(I_f + I_b) = n\ (x_{LiNTf2}/x_{ZI})$ The amount of Li bound increased with of increasing ZI salt concentration. The calculated solvation number decreased from ca. 3 to

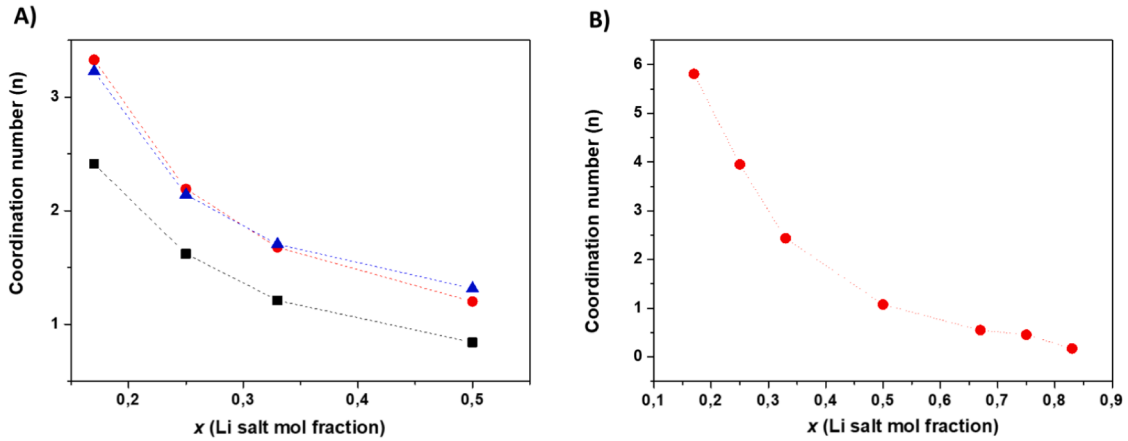

Fig. 3. Coordination number obtained by Raman peaks of the corresponding ZI-$LiNTf_2$ mixtures. A) $I_b/(I_f + I_b) = n\ (x_{LiNTf2}/x_{ZI})$, I_f is the intensity of the free of S═O peak centred at 615, 658 and 697 cm^{-1}, and I_b is the intensity of the bound of S═O peak centred at 623, 677 and 705 cm^{-1}. B) $Ac/(A_c + A_f)$,. A_f is the integrated area of the free NTf_2 peak centred at 742 cm^{-1}, and A_c is the integrated area of the bound NTf_2 peak at ~748 cm^{-1}.

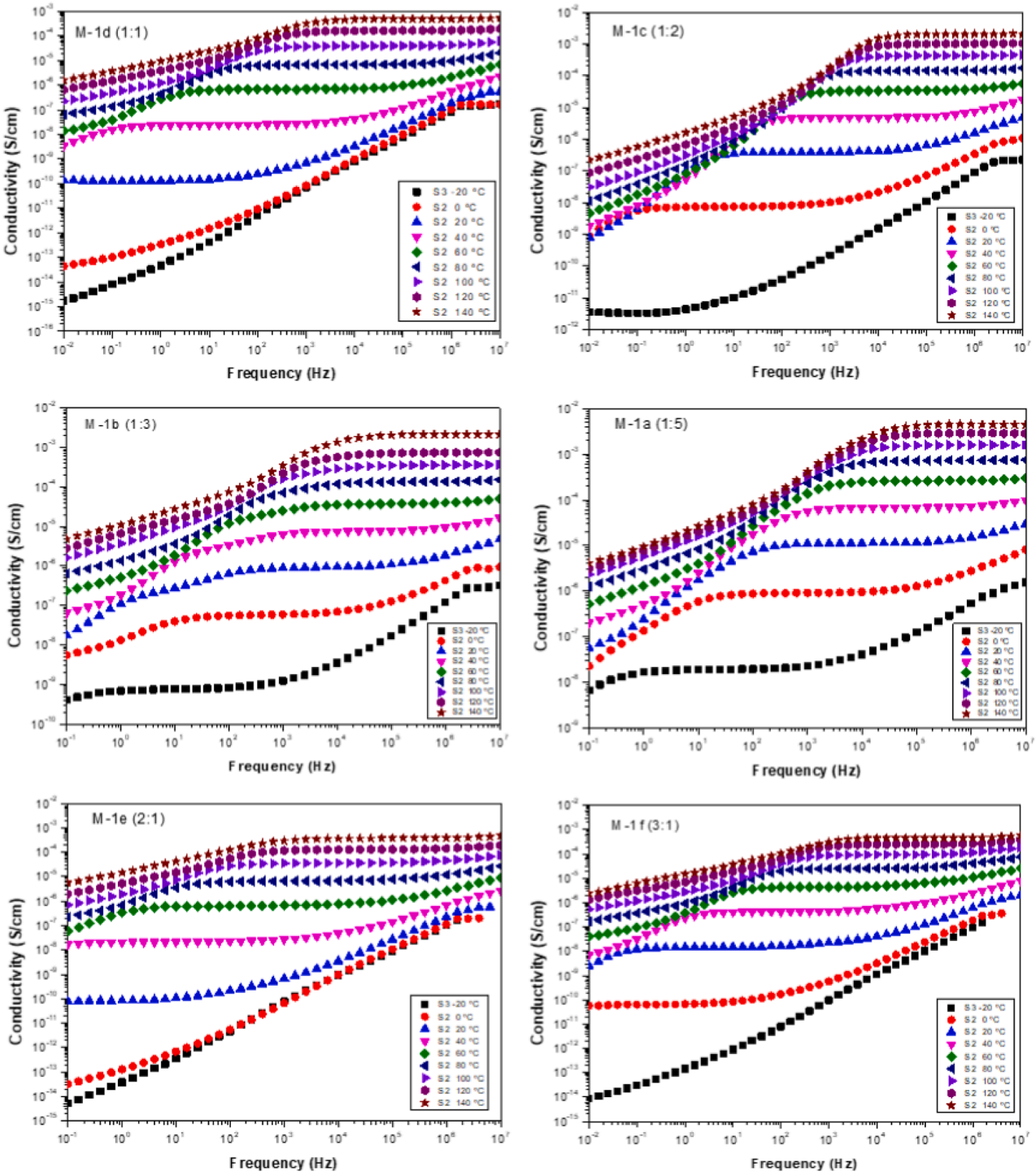

Fig. 4. Conductivity of the **DMSO-ZI-1**:NTf_2 samples in the temperature range compress between −20 °C and 140 °C in steps of 20 °C.

1 when the amount of Li^+ is increased.

On the other hand, the band at ~742 cm^{-1}, which was assigned to the CF_3 bending vibration, combined with that of the S — N stretching vibration of NTf_2^- is also observed. This peak shifts at a higher wavenumber with the increase of the $LiNTf_2$ in the mixture as this mode is sensitive to the interactions of the anion with its local environment [15,16]. This upward shift can be assigned to the anion bound to the metal cation when the corresponding metal NTf_2^- salt is dissolved in the eutectic mixture. The band appearing at 748 cm^{-1} can be attributed to the contact ion pair formation with the NTf_2 anion coordinated to a single Li cation, or to aggregates, where the anion is coordinated to more than one Li cation. Thus, again the position of this peak allows us to assess the "free" or "coordinate" state of the NTf_2 anion with the Li cation. In this case, it is possible to perform the deconvolution of this signal using a Voigt profiles obtaining the area for the "*free*" anion (A_f) and of coordinated species (A_c). With these values is possible to determine the coordination number *n* of Li by taking into account the Li mole fraction × against the integral ratio $A_c/(A_c + A_f)$. The value of *n* can be deduced from $A_c/(A_c + A_f) = n \times {}_{(Li+)}$ [17]. If each lithium ion is assumed to be coordinated by *n* NTf_2^- anions, the concentration of these

anions, which are responsible for the 748 cm^{-1} components, is given by $C_c = nxC_T$, where C_T is the total molar concentration of the NTf_2^- anions. It follows that $A_c = KS_{748}nxC_T$, where K is a proportionality constant and S_{748} is the molar Raman scattering coefficient of the considered component. Similarly, the concentration of free NTf_2^- anions, which are responsible for the 742 cm^{-1} components, is $C_f = C_T - nxC_T$. Hence, $A_f = KS_{742}(C_T - nxC_T)$. By setting $S_{748}/S_{742} = S$, it is easy to deduce that $A_c/(A_c + A_f) = Snx/(Snx - nx + 1)$ assuming a molar Raman scattering coefficient Raman scattering coefficients for free- and bound NTf_2 anion are comparable, then $S \approx S_c/S_f = 1$ and the ratio $A_c/(A_c + A_f)$ can be used to calculate the coordination number for a given eutectic composition. Fig. 3 shows how the coordination number change with the composition of the mixture. This value drastically decreases from *ca.* 5.5 to around 0.5 in the Li salt high concentrated mixtures.

When the concentration of the ZI increases its interaction with Li allows the exchange of the NTf_2^- of the Li-salt by the tethered sulfonic group of the ZI together with the solvation with the S═O group. At a higher molar ratio of ZI, the ZI anions start to participate in the complex formation of Li^+ contact ion-pairs (CIPs), where the anions directly interact with the cation, and aggregates, due to the high electron-pair-donating ability of S═O of the ZI and its stronger affinity toward Li^+. This stronger interaction between Li^+ and S═O of the ZI in comparison with the Li^+ and NTf_2^- results in scarce participation of the NTf_2^- anion in coordinating to Li^+ when the concentration of the ZI is increased leading to separated ion pair between them, where NTf_2^- is not involved in the first solvation shell of Li^+.

2.1. Impedance spectroscopy measurements

Initially, the eutectic mixtures **M-1a-f** were molded by heated them up to 100 °C to get fluid from the semi-solid samples enabling to introduce into a Teflon mold consisting of a 100-μm-thick sheet with a circular hole of with 8.3 mm of diameter. The mold and sample are then placed between two parallel flat electrodes to proceed with the impedance measurements. The experiments were carried out for all mixtures in the interval of temperature compress between −20 °C to 150 °C to obtain the conductivity. To ensure the reproducibility of the results, measurement sweeps were carried out by raising the temperature up to 150 °C, lowering it to −20 °C and raising it back to 150 °C. These sweeps were made in 5 °C isothermal steps. In each of them, 5 measurements per decade were taken in the descending range of frequencies between 10 MHz and 10 mHz.

The experimental data obtained at Novocontrol for the mixtures were analyzed in terms of the complex dielectric permittivity function, $\varepsilon^*(\omega,T)$, and the complex conductivity $\sigma^*(\omega,T) = j\,\omega\,\varepsilon_0\,\varepsilon^*(\omega,T)$, where j is the imaginary unity, ε_0 is the vacuum permittivity and ω the angular frequency of the applied electric field ($\omega = 2\pi f$). From the relationship between the complex dielectric permittivity $\varepsilon^*(\omega,T)$, and complex conductivity $\sigma^*(\omega,T)$; the dc-conductivity (σ_{dc}) can be obtained using three different procedures [18]. i) From the complex dielectric measurements. Where the direct current conductivity (σ_{dc}) can be calculated from the imaginary part of the permittivity, when the Maxwell–Wagner–Sillars (MWS) [19,20] conditions are met, concisely when the bulk conductivity dominates as for pure Ohmic conduction ($\sigma' = \sigma_{dc}$), with $\varepsilon'' = \sigma_{dc}/(\varepsilon_0\omega)$ where ε_0 represents the vacuum permittivity and ω the angular frequency of the applied electric field. This can be seen by the fact that the plot of log(ε") versus log(ω) yields a straight line with slope ≅ −1 over an extended range in the region of high frequency. ii) Another method to determine the σ_{dc} is by means of the Nyquist diagrams, where the imaginary part is plotted versus the real part of impedance (−Z" *vs* Z') [21,22].

iii) And finally, the third method to obtain the σ_{dc} is from the Bode diagram [23].In this work data for the real part of the conductivity in dry conditions were analyzed using the later approach by means of the corresponding Bode diagrams in which the conductivity (in S cm^{-1}) versus frequency (in Hz) is plotted for all ranges of temperatures. Fig. 4

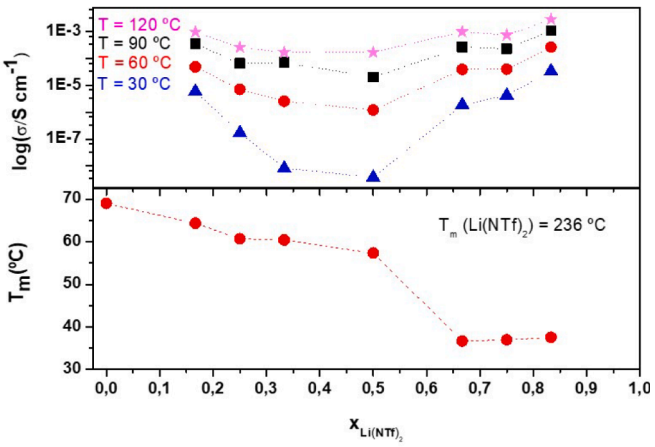

Fig. 5. Effect of added LiTFSI on the ionic conductivity and Tm of DES salt **1**, at different temperatures: 30, 60, 90 and 120 °C.

shows these Bode diagrams for the different mixtures analyzed from −20 °C to 140 °C in steeps of 20 °C, respectively. On the other hand, Figure SI5 shows the variation of the phase angle (ϕ) versus frequency at the same temperatures. A closer inspection of both figures reveals that conductivity tends to a constant value (plateau) when the phase angle (ϕ) tends to zero or to a maximum. Besides, a section where the conductivity decreases when the frequency decreases was observed. A transition zone was also observed in the range of 10^4 to 10^1 Hz, depending on the mixture composition and temperature. The first process is directly related with the resistance/stability of the sample and the second process is related to the diffusion (charge transfer) due to the mobility of the NTf_2 anions as a consequence of the electrode polarization [24,25]. The reported values of the conductivity were obtained from the plateau at the frequency where the phase angle was practically zero.

The change in σ_{dc} of the different samples at different temperatures is observed and can be extracted from the plateau in the high-frequency range. Furthermore, the frequency value where the plateau is reached is shifted to higher frequencies by increasing the temperature because of the thermal activation of ionic liquid NTf_2^- transport. For example, Fig. 5 shows, at 30 °C, the conductivity values followed the trend: $\sigma_{LZW\text{-}NTf2}$ (**M−1d**) (3. 7 × 10^{-9} S cm^{-1}) < $\sigma_{LZW\text{-}NTf2}$ (**M−1e**) (4.1 × 10^{-9} S cm^{-1}) < $\sigma_{LZW\text{-}NTf2}$ (**M−1f**) (1.7 × 10^{-7} S cm^{-1}) < $\sigma_{LZW\text{-}NTf2}$ (**M−1c**) (1.9 × 10^{-6} S cm^{-1}) < $\sigma_{LZW\text{-}NTf2}$ (**M−1b**) (4.2 × 10^{-6} S cm^{-1}) < $\sigma_{LZW\text{-}NTf2}$ (**M−1a**) (3.4 × 10^{-5} S cm^{-1}). Similar trends can be observed for the other temperatures studied (for example, 60 °C, 90 °C and 120 °C). For 120 °C the conductivity values obtained, follow the trend, $\sigma_{LZW\text{-}NTf2}$ (**M−1d**) (1. 7 × 10^{-4} S cm^{-1}) ≅ $\sigma_{LZW\text{-}NTf2}$ (**M−1e**) (1.7 × 10^{-4} S cm^{-1}) < $\sigma_{LZW\text{-}NTf2}$ (**M−1f**) (2.6 × 10^{-4} S cm^{-1}) < $\sigma_{LZW\text{-}NTf2}$ (**M−1b**) (7.4 × 10^{-4} S cm^{-1}) < $\sigma_{LZW\text{-}NTf2}$ (**M−1c**) (1.0 × 10^{-3} S cm^{-1}) < $\sigma_{LZW\text{-}NTf2}$ (**M−1a**) (2.9 × 10^{-3} S cm^{-1}), respectively.

These differences in conductivity with the composition can be associated with the concentration of the mobile anions ($LiNTf_2$) and their mobility associated with the strength of the interactions with the different stages of the mixtures at these temperatures. The DSC studies reveal that the mixtures containing a larger molar mass of $LiNTf_2$ (x($LiNTf_2$) ≥ 0.7 (M-1a and M1-b) displayed lower glass transitions (T_m = 37.5 and 36.9 °C, Fig. 5, Table 1 and **Figure SI.3**), while those more reach in zwitterionic salt (x(**DMSO-**ZIs-1) > 0.3. M-1d and M-1f) present melting points higher than 50 °C increasing from 57.9 up to 64.3 with the increase of the zwitterionic salt (Table 1 and Figure SI.3). Thus, bellow the T_m the mixtures present lower conductivity than temperatures above the T_m of the mixtures. The ionic conductivity of the mixtures with higher lithium salt displays higher values (i.e. σ (**M-1a**) **DMSO-ZI-1**:NTf_2 2.9 × 10^{-3} S cm^{-1}). On the other hand, the

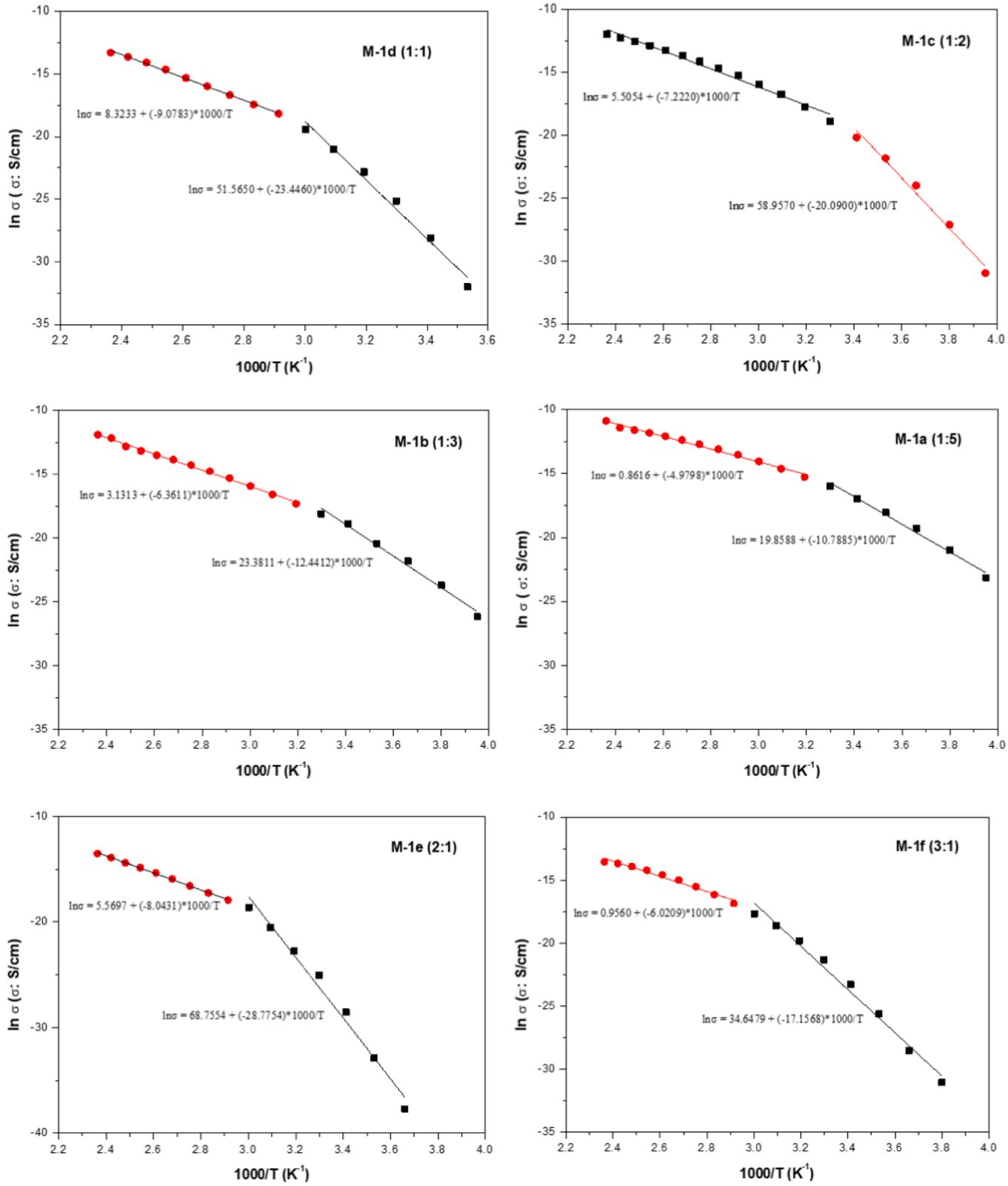

Fig. 6. Arrhenius plot of the LZW-NTf_2 samples in the entire temperature range compress between −20 °C and 150 °C in steeps of 10 °C.

conductivity of mixtures with higher content of zwitterion (**M-1d**, **M-1e** and **M-1f**) was smaller than those with higher $LiNTf_2$ content, two or three orders of magnitude at low temperatures and about one order of magnitude at high temperatures. These results suggest that the plasticity effect of the NTf_2 anion significantly governs the high ionic conductivity of zwitterionic-type materials. The frequency range for the highest values of conductivity is compressed between 10^4 to 10^6 Hz in the sample at higher temperatures and at low frequencies in the interval of temperatures compress between −20 °C and 70 °C, depending on NTf_2^- content. Furthermore, the conductivity in that frequency range (high

Table 2
Activation energy calculated from the fit below and above the melting temperature for all the mixtures.

Entry	Sample	E_{act} (below T_m)	E_{act} (above T_m)	$T_{m\ (A.p.)}$ [a] (°C)	$T_{m\ (DSC)}$ [b] (°C)
1	**M-1a** (1-5)	90 ± 5	41.6 ± 1.3	35 ± 1	37.5 ± 0.1
2	**M-1b** (1-3)	103 ± 6	53 ± 1	34 ± 1	36.9 ± 0.1
3	**M-1c** (1-2)	167 ± 12	60 ± 2	31 ± 1	36.4 ± 0.1
4	**M-1d** (1-1)	195 ± 12	75.5 ± 1.4	55 ± 1	57.3 ± 0.2
5	**M-1e** (2-1)	199 ± 13	66.8 ± 1.0	60 ± 1	60.4 ± 0.1
6	**M-1f** (3-1)	143 ± 6	50 ± 3	62 ± 1	60.7 ± 0.1

[a] $T_{m\ (A.p.)}$ is the melting temperature observed by Arrhenius's behavior in conductivity.
[b] $T_{m\ (DSC)}$ is the melting temperature obtained by DSC.

frequencies) is practically constant; as we can see from Fig. 4, and this behaviour is related to a good interaction of ZI with the NTf_2. The variation in conductivity with the NTf_2^- loading can be rationalized by two factors. One of them is the concentration of the mobile anions, and the other is their mobility associated with the strength of the intermolecular interactions between the species present in the mixture.

These results are like those observed by Yoshizawa et al. for other functionalized ZI – $LiNTf_2$ mixtures, where the conductivity was 3.8 × 10^{-4} S cm^{-1} at 80 °C [3,6]. The introduction of task-specific functional groups (i.e. ether bonds) to zwitterions clearly affects the ionic conductivity. Furthermore, they reported a clear effect of the Li-salt concentration. For salt-in-zwitterion concentration range, the ionic conductivity of the composites is ~10^{-5} S cm^{-1} at 40 °C. In contrast, in the zwitterion-in-salt concentration range, the ionic conductivity decreased upon the increase in the Li-salt concentration, except for 80 mol%. The dependence of the ionic conductivity of the **ZI**/Li-salt composites on the salt concentration is consistent with the dependence of melting on the concentration of the salt.

From the plot shown in Fig. 6, we observe that the dc-conductivity of all mixtures increases with temperature increase. For the thermal activation energy, two clearly different Arrhenius trends are observed. For all the mixtures the temperature where the slope of the Arrhenius plot changes is on the range of the melting temperature experimentally observed for the mixture (Fig. 6). The values of the activation energy calculated from the slopes below and above melting temperatures are given in Table 2. Below the melting temperature, the values of activation energy are around of two times higher than the values observed for all the mixtures above the melting temperature. In Table 2, we can see the activation energy obtained in each one of the mixtures below and above melting temperature together with the temperature where the slope of the Arrhenius plot changes. The calculated activation energy for the mixtures in the interval of temperatures compress between −20 °C and the melting temperatures follow the trend E_{act} (**M-1d**) ≅ E_{act} (**M-1e**) > E_{act} (**M-1c**) > E_{act} (**M-1f**) > E_{act} (**M-1b**) > E_{act} (**M-1a**), respectively. These values are higher than the activation energy obtained for the temperatures above melting temperature, where the activation energy follows the trend E_{act} (**M-1d**) > E_{act} (**M-1e**) > E_{act} (**M-1c**) > E_{act} (**M-1b**) > E_{act} (**M-1f**) > E_{act} (**M-1a**), respectively.

2.2. Diffusion coefficients and ionic charge concentration

The parameters more important to characterize and estimate in ionic transport are the mobility and the total charge carrier concentration, however, they are in general difficult to quantify. Many investigations have been carried out trying to obtain equations that allow giving some approximate information to the experimental results, in order to determine the ion diffusion coefficient, the complex permittivity and the ionic charge concentration, under an applied electric field. [16,20,24–35]. Some of them use a generalization of the theory of Trukhan [36] following the Nernst-Planck electrodiffusion equations linearized for the dielectric dispersion caused by the electrodiffusion of ions in the mixtures confined between two electrodes [17,18,30,31].

When the maximum in tan δ is not seen, there is difficult to determine the parameter κ_L, where κ is the inverse of Debye length and L the sample thickness. However, in some cases, we may use the fact that the specific conductivity, σ, can be determined easily from measurements of Bode or Nyquist diagrams. In the region of frequencies where the Maxwell-Wagner-Sillars (MWS) effect is dominant over effects of surface polarization (low frequencies) and internal relaxations in the polymer (high frequencies) the MWS permittivity can be expressed as [20,21]:

$$\varepsilon^*_{MWS} = \frac{\kappa L \cdot \varepsilon_s}{j\Omega\zeta_{MWS}} = \varepsilon_s\left[1 + \frac{M}{j\Omega}\right] \quad (1)$$

Where ε_s is the static permittivity, $\zeta_{MWS,film}$ is the dimensionless Maxwell-Wagner-Sillars film impedance, and $\Omega = \omega\cdot\kappa^{-2}\cdot\frac{1}{\sqrt{D_1 D_2}}$. Eq. (1) we can transformed in the familiar expression:

$$\varepsilon^*_{MWS} = \varepsilon^*_s + \frac{\sigma}{j\omega} = \frac{L}{j\omega Z_{MWS}} \quad (2)$$

Where,

$$\sigma = \varepsilon_s\kappa^2\left[\frac{\nu_+ z_+^2 D_+ + \nu_- z_-^2 D_-}{\nu_+ z_+^2 + \nu_- z_-^2}\right] \quad (3)$$

To obtain the true contribution of each ion into ionic transport in polymerized ionic liquids and their mixtures is not an easy task. For this will be necessary to know the respective roles of cations and anions in the mixtures from conductivity measurements. How this conductivity is obtained for all the system, this is the sum of the contributions of total charge mobile, i.e., σ = σ+ + σ−. For this, although all the available charges participate in the ionic transport, we are assumed in our study that the highest contribution plausible to the true conductivity, $\sigma = \sigma_{dc}$, in all our samples, is the mobility of the anions because the zwitterion is practically suppressed [3]. Therefore, we can calculate the diffusion coefficient from the conductivity measurements assuming that this is only associated to the contributions of anions ($D_- = D$). Then equation (3) can be transformed as:

$$\sigma = \varepsilon_s\kappa^2\frac{D_-}{2}\left[\frac{D_+}{D_-} + 1\right] \cong \varepsilon_s\kappa^2\frac{D}{2} \quad (4)$$

When the values of the inverse Debye length can be obtained from the peaks of loss tangent or from the maximum in ε" which is often difficult to observe, we can estimate the values of ε_s. Our composites formed by functionalized Zwitterionic ILs and $LiNTf_2$ were treated as one salt, at different concentrations of ZI and $LiNTf_2$, respectively.

In such systems, the ions are not separated by solvent molecules, and hence, there are always in contact. Then, these mixtures may be regarded as media where the ions are completely distributed, and the only interaction is of type ion-ion. However, independently of the theory used in the description of ionic conduction, an addition of Il to an ionic liquid, should result in the modification of ion-ion interactions, to different ionic species present in the system such is also observed by other researchers in the study of the conductivity of different mixtures between ionic liquids (ILs) and molecular liquids (ML). In such mixtures, has been observed that the specific conductivity increases monotonically on the composition of the mixture [37]. In our study, we are supposed to neglect ion-ion interactions and the electroneutrality at the equilibrium condition is satisfied for the mixed of the sample. Then, we have $n_+(eq) = n_-(eq) = n$. For such suppositions, the inverse Debye length in the mixed ZI/$LiNTf_2$ (x:y) can be written as:

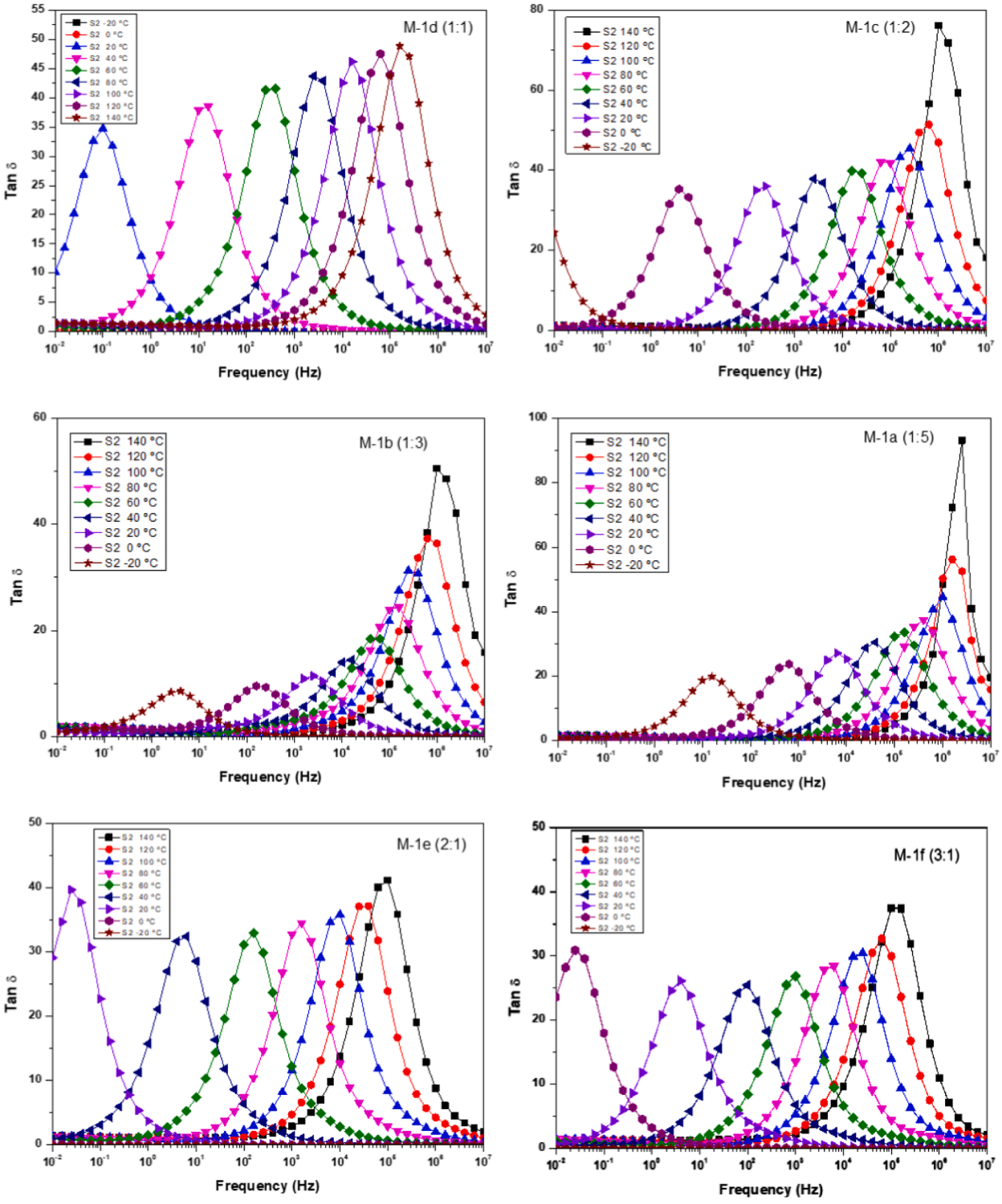

Fig. 7. Los tangent for all the sample Zw/$LiNTf_2$ (x:y) in all the range of temperatures in steeps of 20 °C.

$$\kappa^2 = \frac{2F^2 c_s}{RT\varepsilon_s} \tag{5}$$

combining equations (4) and (5) we may calculate the mobile charge concentration n as:

$$n = \frac{RT}{F^2}\frac{\sigma}{D} \tag{6}$$

Where R is the gas constant, T is the absolute temperature, F is the Faraday's constant, σ the dc-conductivity of the samples, and D is the diffusion coefficient of the anions (D = D_).

The equation (6) permits us to determine the concentration of charge carriers from the values of the ionic dc-conductivity measured from the high-frequency domain where the loss tangent reaches a maximum in the dielectric spectra, a value that is determined knowing the diffusion coefficient according to the equation (**A16. See appendix**).

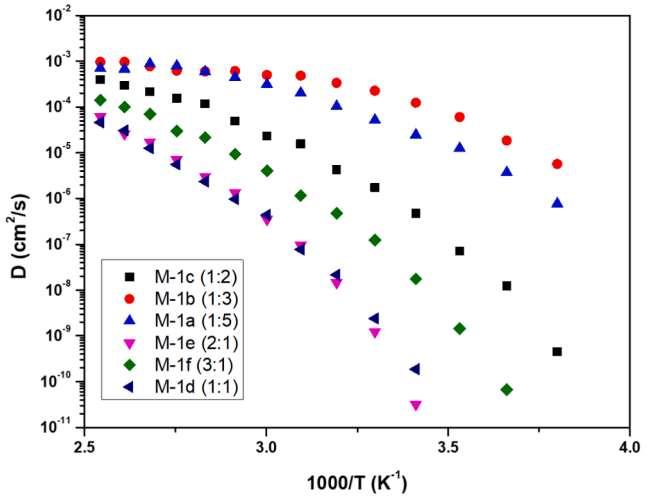

Fig. 8. Temperature dependence of diffusion coefficient of the samples in all the range of temperatures studied.

$$D = \frac{\omega_{max}^{\tan\delta} \cdot L^2}{32(\tan^3\delta)_{max,\omega}} \quad (7)$$

Fig. 7 shows the experimental results for tan δ as a function of the perturbation frequency for all the samples at different temperatures from −20 °C to 140 °C in steeps of 20 °C.

As we can see in Fig. 7 a clear peak in *Tan* δ is observed for all the samples from −20 °C to 140 °C to shift towards higher frequencies, increasing their value at the peak as the temperature increases, which is associated with the plateau of the real part of the conductivity observed in the Bode diagrams (see Fig. 4). This maximum always shifts to higher frequencies increasing in intensity as a function of temperature. Some differences, however, are observed for the different mixtures. As we can see for the samples **M-1c** and **M-1b**, the increase in the temperature produces a growth in maximum intensity with respect to the samples **M-1e** and **M-1f** where the melting temperature and the amount of $LiNTf_2$ is higher. On the other hand, a close inspection of these figures shows that samples **M-1c**, **M-1b** and **M-1a** are louder and more shifted towards high frequencies than samples **M-1e** and **M-1f**, respectively. That's means that the amount of $LiNTf_2$ is the true responsible for increasing the conductivity in the samples.

The diffusivity values (*D*) obtained using equation (10) are shown in Fig. 8 as a function of the temperature. From this figure, a diffusivity effect like the one observed in conductivity is esteemed. From the analysis of our results, we can observe that diffusivity can be affected by interactions between the two ILs depending on their concentrations.

We can notice that the diffusivity of Zw/$LiNTf_2$ (1:X) with (X = 2, 3 and 5) is higher than Zw/$LiNTf_2$ (Y,1) where (Y = 1, 2 and 3). On the other hand, a strong change in diffusivity with temperature is clearly observed for all Mixtures of **DMSO-**ZIs-1 with different molar ratios of $LiNTf_2$, where the corresponding diffusion coefficients have an anomalous temperature variation, particularly it is more appreciated below 100 °C, where the activation energy is very much higher than at high temperature, up to 100 °C. This variation is closely related to the density of charge carriers existing in the mixture, and possibly due to both the anion binding energies and stabilization energy. A close inspection of diffusion coefficient variation shows that a decrease in the coefficient of diffusion is observed for Zw/$LiNTf_2$ (Y,X) when X → Y.

The free ion density can be obtained from the dc-conductivity and diffusion coefficient according to the Einstein relation considering that the valence of cation and anion are the same and the mobility of both ions are quite similar, then the total charge carrier density can be calculated from equation (9). Where we have supposed that in our study the dissociation-association dynamics are satisfied completely being much faster than the macroscopic electrode polarization.

Fig. 9 displays mobile ion concentrations in agreement with equation (9). The obtained values are very different depending on the amount of IL of each mixture, varying practically linearly for the mixed **M-1c**, **M-1b** and **M-1a** while in the case of the mixed **M-1e** and **M-1f** like the behaviour observed in conductivity. Both behaviours tend to have a fixed value at high temperatures around of $5x10^{24}$ m^{-3}. This value is within 20–30 % of the expected value. On the other hand, the

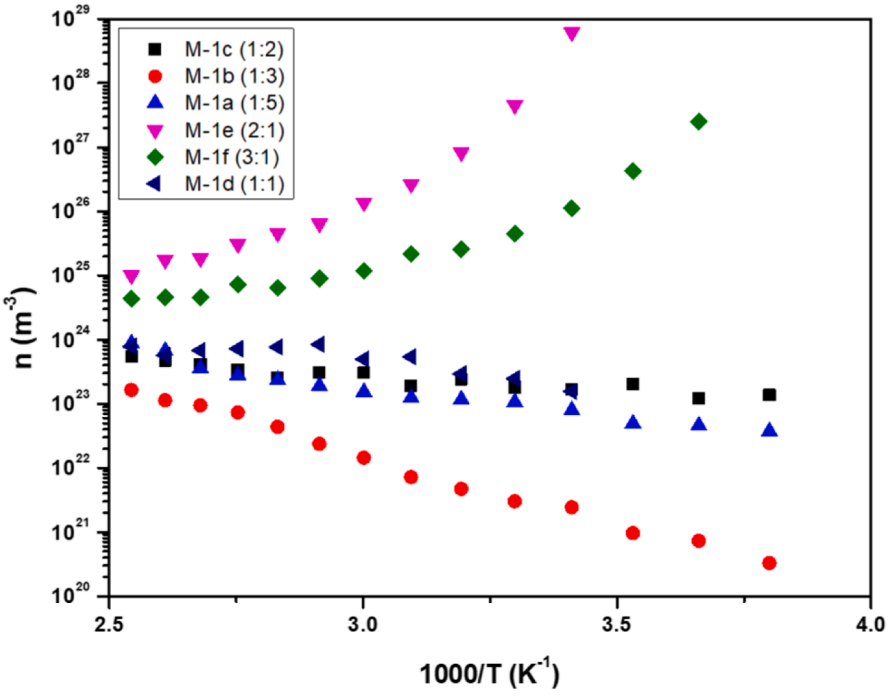

Fig. 9. Temperature dependence of the ionic charge density for all the mixtures in the entire range of temperatures.

dependence with temperature of diffusion coefficient and charge carrier density of the mixed revealed that the abrupt change observed for the conductivity between 40 and 80 °C depending on the mixed is dominated by a charge carrier density, such is observed *n* in Fig. 9. This is a typical behaviour also observed in the crystalline melting samples.

Quantifying the real value of the ionic carrier density in a system where there are many parameters which have influence on the process is a difficult task and the values are always subject to the model used for their determination, as well as the approximations made to simplify the mathematical calculation [38–40]. The results found for the mixtures **M-1e** and **M-1f** show a diminution of free charge density when the temperature increases. It could be possible due to the strong electrostatic interaction between ion pairs and mobile anions the formation of transient pairs $Li^{+\cdots}NTf_2$ in case of these type of mixtures. However, in the case of the mixtures Zw/$LiNTf_2$ (1:X) with (X = 2, 3 and 5) this behaviour is very different where an increase in charge carriers density when the temperature increase was observed being this behaviour practically linear with the reciprocal of the temperature. Therefore, our results showed in Fig. 9 are subject to the model used and the approximations made, since our results can be described approximately by a simple Debye relaxation. In the case that dielectric properties could not be described by means of a simple Debye, will be convenient to use different models described by Cole-Cole and Havriliak-Negami equations [30–32,41–43]. In such circumstances the analysis on carrier's density based on electrode polarization can over-estimates the effective dissociated ion density respect the stoichiometric concentration such as previously have been evidenced in membranes containing ILs [23,30–32,44,45].

3. Conclusions

In this study, we have designed a series of Zweterions ionic liquids functionalized with methyl sulfoxide moieties. As far as we are aware, the use of these functionalized zwitterionic combining both the zwitterionic unit and de S═O that can further solvate the Li cations to modulate the ionic conductivity of mixtures of ZI and lithium slats has never reported before. This task-specific zweterions form low temperature eutectic mixtures with $LiNTf_2$ we observed that in the mixtures the lithium cation is less coordinated to the NTf_2 anions by intermolecular interactions of the zwitterionic salt with the $LiNTf_2$ through hydrogen bonding. These interactions are likely to be responsible of the reduction in melting. The Raman studies reveal a different Li+ coordination number depending on the molar mixture composition. The competition between the S═O of the NTf_2 anion and the dimethylsufoxide units of the ZILs results in a different coordination of the lithium with weaker ion paring compared to $LiNTf_2$.

The ionic conductivity of these mixtures is mainly governed by the interaction between both ionic components, especially the cationic moiety of ZI with the anion of the added salt. Our conductivity values follow the trend: $\sigma_{LZW\text{-}NTf2}$ (**M-1d**) < $\sigma_{LZW\text{-}NTf2}$ (**M-1e**) < $\sigma_{LZW\text{-}NTf2}$ (**M-1f**) < $\sigma_{LZW\text{-}NTf2}$ (**M-1c**) < $\sigma_{LZW\text{-}NTf2}$ (**M-1b**) < $\sigma_{LZW\text{-}NTf2}$ (**M-1a**) in all the range of temperatures studied. In the interval of temperatures compress between -20 °C and the melting temperatures the activation energy calculated from an Arrhenius behavior follows the trend E_{act} (**M-1d**) ≅ E_{act} (**M-1e**) > E_{act} (**M-1c**) > E_{act} (**M-1f**) > E_{act} (**M-1b**) > E_{act} (**M-1a**), respectively. These values are higher than the activation energy obtained for the temperatures above melting temperature, where the activation energy follows the trend E_{act} (**M-1d**) > E_{act} (**M-1e**) > E_{act} (**M-1c**) > E_{act} (**M-1b**) > E_{act} (**M-1f**) > E_{act} (**M-1a**), respectively.

Using a generalization of the theory of Trukhan the diffusivity and charge carriers density, have been calculated for each mixed of ILs. Our results, observed with the caution of the model and suppositions usedshowed for the diffusivity a similar behaviour to the conductivity where the diffusion coefficient in each mixed can be affected by interactions between the two ILs depending on its concentrations being the diffusivity of Zw/$LiNTf_2$ (1:X) with (X = 2, 3 and 5) is higher than Zw/$LiNTf_2$ (Y,1) where (Y = 1, 2 and 3).

Finally, the temperature dependence of the diffusion coefficient and charge carrier density of the mixed revealed that the abrupt change observed for the conductivity between 40 and 80 °C depending on the mixed is dominated by a charge carrier density.

Although the introduction of the methyl sulfoxide functionality onto the zwitterion caused an increase in Tm for the corresponding ionic mixture, they present reasonable low-temperature melting points and good thermal stability (>200 °C) with interesting conductivity properties for the development of different electrochemical applications.

CRediT authorship contribution statement

Daniel Nuevo: Conceptualization, Investigation, Methodology. **Marc Cuesta:** Conceptualization, Investigation, Methodology. **Raul Porcar:** Methodology, Visualization, Data curation, Investigation. **Andreu Andrio:** Investigation, Methodology, Supervision, Validation, Data curation. **Eduardo Garcia-Verdugo:** Visualization, Supervision, Validation, Conceptualization, Funding acquisition, Writing – review & editing. **Vicente Compañ:** Investigation, Methodology, Visualization, Supervision, Validation, Conceptualization, Funding acquisition, Writing – review & editing.

Declaration of Competing Interest

The authors declare that they have no known competing financial interests or personal relationships that could have appeared to influence the work reported in this paper.

Data availability

Data will be made available on request.

Acknowledgment

We want to acknowledge PDC2022-133313-C22 by MCIN/AEI /10.13039/501100011033 and by European Union Next Generation EU/ PRTR, Ministerio de Economía y Competitividad Grant Number PID 2019-107137 RB-C21, and by Ayudas investigadores tempranos UNED-Santander (2022V/ITEMP/001). The authors are grateful to the SCIC of the Universitat Jaume I for technical support.

Appendix A. Supplementary material

Supplementary data to this article can be found online at https://doi.org/10.1016/j.chemphys.2023.112043.

References

[1] A. Wu, Y. Gao, L. Zheng, Zwitterionic amphiphiles: their aggregation behavior and applications, Green Chem. 21 (2019) 4290–4312.
[2] H. Ohno, M. Yoshizawa-Fujita, Y. Kohno, Design and properties of functional zwitterions derived from ionic liquids, Phys. Chem. Chem. Phys. 20 (2018) 10978–10991.
[3] M. Yoshizawa, M. Hirao, K. Ito-Akita, H. Ohno, Ion Conduction in Zwitterionic-Type Molten Salts and Their Polymers, J. Mater. Chem. 11 (2001) 1057–1062.
[4] B. Byrne, P.C. Howlett, D.R. MacFarlane, M. Forsyth, The Zwitterion Effect in Ionic Liquids: Towards Practical Rechargeable Lithium-Metal Batteries, Adv. Mater. 17 (2005) 2497–2501.
[5] A. Narita, W. Shibayama, H. Ohno, Structural Factors to Improve Physico-Chemical Properties of Zwitterions as Ion Conductive Matrices, J. Mater. Chem. 16 (2006) 1475–1482.
[6] M. Yoshizawa-Fujita, H. Ohno, Applications of zwitterions and zwitterionic polymers for Li-ion batteries, Chem. Rec. 23 (8) (2023) e202200287, https://doi.org/10.1002/tcr.202200287.
[7] Z. Zhang, P. Zhang, Z. Liu, B. Du, Z. Peng, A Novel Zwitterionic Ionic Liquid-Based Electrolyte for More Efficient and Safer Lithium-Sulfur Batteries, Mater. Interfaces 12 (10) (2020) 11635–11642.
[8] S.-g. Lee, Functionalized imidazolium salts for task-specific ionic liquids and their applications, Chem. Commun. (10) (2006) 1049.

[9] A.D. Sawant, D.G. Raut, N.B. Darvatkar, M.M. Salunkhe, Recent developments of task-specific ionic liquids in organic synthesis, Green Chem. Lett. Rev. 4 (2011) 41–45.

[10] M.-N. Roy, J.C. Poupon, A.B. Charette, Tetraarylphosphonium Salts as Soluble Supports for Oxidative Catalysts and Reagents, J. Org. Chem. 74 (2009) 8510–8515.

[11] D. Tsuchiya, M. Tabata, K. Moriyama, H. Togo, Efficient Swern oxidation and Corey-Kim oxidation with ion-supported methyl sulfoxides and methyl sulfides, Tetrahedron 68 (2012) 6849–6855.

[12] M. Yoshizawa, A. Narita, H. Ohno, Design of Ionic Liquids for Electrochemical Applications, Aust. J. Chem. 57 (2004) 139–144.

[13] X. Xuan, J. Wang, Y. Zhao, J. Zhu, Experimental and computational studies on the solvation of lithium tetrafluorobrate in dimethyl sulfoxide, J. Raman Spectrosc. 38 (2007) 865–872.

[14] A.R. Neale, R. Sharpe, S.R. Yeandel, C.-H. Yen, K.V. Luzyanin, P. Goddard, E. A. Petrucco, L.J. Hardwick, Design Parameters for Ionic Liquid-Molecular Solvent Blend Electrolytes to Enable Stable Li Metal Cycling Within Li-O2 Batteries, Adv. Funct. Mater. 31 (2021) 2010627.

[15] J.C. Lassegues, J. Grondin, D. Talaga, Lithium solvation in bis (trifluoromethanesulfonyl)imide-based ionic liquids, Phys. Chem. Chem. Phys. 8 (2006) 5629–5632.

[16] Y. Umebayashi, T. Yamaguchi, S. Fukuda, T. Mitsugi, M. Takeuchi, K. Fujii, S. Ishiguro, Raman Spectroscopic Study on Alkaline Metal Ion Solvation in 1-Butyl-3-methylimidazolium Bis(trifluoromethanesulfonyl)amide Ionic Liquid, Anal. Sci. 24 (2008) 1297–1304.

[17] J.-C. Lassègues, J. Grondin, C. Aupetit, P. Johansson, Spectroscopic Identification of the Lithium Ion Transporting Species in LiTFSI-Doped Ionic Liquids, J. Phys. Chem. A 113 (2009) 305–314.

[18] J. Escorihuela, R. Narducci, V. Compañ, F. Costantino, Review: Proton Conductivity of Composite Polyelectrolyte Membranes with Metal-Organic Frameworks for Fuel Cell Applications, Adv. Mater. Interfaces 6 (2) (2019) 1801146, https://doi.org/10.1002/admi.201801146.

[19] T.S. Sørensen, V. Compañ, Complex permittivity of a conducting, dielectric layer containing arbitrary binary Nernst-Planck electrolytes with applications to polymer films and cellulose acetate membranes, J. Chem. Soc., Faraday Trans. 91 (1995) 4235–4250.

[20] V. Compañ, T.S. Sørensen, R. Diaz-Calleja, Complex permittivity of a film of poly [4-(acryloxy)phenyl-(4-chlorophenyl)methanone] containing free ion impurities and the separation of the contributions from interfacial polarization, Maxwell–Wagner–Sillars effects and dielectric relaxations of the polymer chains, J. Chem. Soc., Faraday Trans. 92 (1996) 1947–1957.

[21] V. Compañ, J. Escorihuela, J. Olvera, A. García-Bernabé, A. Andrio, Influence of the anion on diffusivity and mobility of ionic liquids composite polybenzimidazol membranes, Electrochim. Acta 354 (2020) 136666.

[22] J. Vega-Moreno, A.A. Lemus-Santana, E. Reguera, A. Andrio, V. Compañ, High Proton conductivity at low and moderate temperature in a simple family of Prussian blue analogs, divalent transition metal hexacyanocobaltates (III), Electrochim. Acta 360 (2020), 136959.

[23] D. Valverde, A. Garcia-Bernabe, A. Andrio, E. García-Verdugo, S.V. Luis, V. Compañ, Free ion diffusivity and charge concentration on cross-linked ~ polymeric ionic liquid iongel films based on sulfonated zwitterionic salts and lithium ions, Phys. Chem. Chem. Phys. 21 (2019) 17923–17932.

[24] V. Compañ, T.S. Sorensen, R. Diaz-Calleja, E.R. Riande, Diffusion coefficients of conductive ions in a copolymer of vinylidene cyanide and vinyl acetate obtained from dielectric measurements using the model of Trukhan, J. Appl. Phys. 79 (1996) 403.

[25] R.J. Klein, S. Zhang, S. Duo, B.H. Jones, R.H. Colby, J. Runt, Modeling electrode polarization in dielectric spectroscopy: Ion mobility and mobile ion concentration of single-ion polymer electrolytes, J. Chem. Phys. 124 (2006), 144903.

[26] M. Watanabe, S. Nagano, K. Sanui, N. Ogata, Estimation of Li+ transport number in polymer electrolytes by the combination of complex impedance and potentiostatic polarization measurements, Solid State Ion. (1988) 911–917.

[27] K. Hayamizu, E. Akiba, T. Bando, Y. Aihara, 1H, 7Li, and 19F nuclear magnetic resonance and ionic conductivity studies for liquid electrolytes composed of glymes and polyetheneglycol dimethyl ethers of CH3O(CH2CH2O)nCH3 (n=3–50) doped with LiN(SO2CF3)2, J. Chem. Phys. 117 (2002) 5929–5939.

[28] J. Vega, A. Andrio, A.A. Lemus, L.F. Del Castillo, V. Compañ, Conductivity study of Zeolitic Imidazolate Frameworks, Tetrabutylammonium hydroxide doped with Zeolitic Imidazolate Frameworks, and mixed matrx membranes of Polyetherimide/ Tetrabutylammonium hydroxide doped with Zeolitic Imidazolate Frameworks for proton conducting applications, Elerctrochim. Acta. 258 (2017) 153–166.

[29] G.A. Niklasson, A.K. Jonsson, M. Stromme, Y. Barsoukov, J.R. Macdonald, In Impedance Spectroscopy, 2nd ed, Wiley, New York, 2005, pp. 302–326.

[30] H.J. Schütt, Determination of the free ionic carrier concentration: A discussion of different methods, Solid State Ion. 505 (1994) 70–71.

[31] H.J. Schütt, E. Gerdes, Space-charge relaxation in ionicly conducting oxide glasses. I. Model and frequency response, J. Non-Cryst. Solids 144 (1992) 1–13.

[32] R. Coelho, Physics of Dielectrics for Engineer, 1st. Edition, Elsevier Scientific Publishing Company, New York, 1979, pp. 97–102.

[33] C. Krause, J.R. Sangoro, C. Iacob, F. Kremer, Charge Transport and Dipolar Relaxations in Imidazolium-Based Ionic Liquids, J. Phys. Chem. B 114 (2010) 382–386.

[34] T.M.W.J. Bandara, et al., Quasi solid state polymer electrolyte with binary iodide salts for photo-electrochemical solar cells, Int. J. Hydrog. Energy 39 (6) (2014) 2997–3004.

[35] T.M.W.J. Bandara, M.A.K.L. Dissanayake, I. Albinsson, B.-E. Mellander, Mobile charge carrier concentration and mobility of a polymer electrolyte containing PEO and Pr4N+ I− using electrical and dielectric measurements, Solid State Ion. 189 (2011) 63–68.

[36] E.M. Trukhan, Dispersion of the dielectric constant of heterogeneous systems, Sov. Phys. Solid State 4 (1963) 2560–2570.

[37] A. Jarosik, R. Krajewski, A. Lewandowski, P. Radzimski, Conductivity of ionic liquids in mixtures, J. Mol. Liq. 123 (2006) 43–50.

[38] Y. Wang, C.N. Sun, F. Fan, J.R. Sangoro, M.B. Berman, S.G. Greenbaum, T. A. Zaswodzinski, A.P. Sokoñov, Examination of methods to determine free-ion diffusivity and number density from analysis of electrode polarization, Phys. Rev. E 87 (2013), 042308.

[39] V. Compañ, R. Diaz-Calleja, J. Diaz-Boils, J. Escorihuela, Distribution of relaxation times: Debye Length Distribution *vs.* Electrode Polarization by a Cole-Cole Relaxation Model, J. Electrochem. Soc. 169 (2022), 013506.

[40] A. Serghei, M. Tress, J.R. Sangoro, F. Kremer, Electrode polarization and charge transport at solid interfaces, Phys. Rev. B 80 (18) (2009).

[41] R. Coelho, On the static permittivity of dipolar and conductive media — an educational approach, J. Non. Cryst. Solids 131 (1991) 1136–1139.

[42] F. Kremer, A. Schönhals (Eds.), Broadband Dielectric Spectroscopy, Springer Berlin Heidelberg, Berlin, Heidelberg, 2003.

[43] F. Tian, Y. Ohki, Charge transport and electrode polarization in epoxy resin at high temperatures, J. Phys. D. 47 (2014), 045311.

[44] P.G. Bruce, F.M. Gray, Solid State Electrochemistry, Cambridge University Press, Cambridge, 1995.

[45] D. Fragiadakis, S. Dou, R.H. Colby, J. Runt, Moleculkar mobility, ion mobility, and mobile ion concentration in poly(ethylene oxide)-based polyurethane ionomers, Macromolecules 41 (2008) 5723–5728.